Journal of Molecular Structure 1319 (2025) 139585

Contents lists available at ScienceDirect

Journal of Molecular Structure

journal homepage: www.elsevier.com/locate/molstr

The experimental and DFT approaches on electronic, thermal and conductivity properties of non-linear optical bearing fused aromatic chalcones towards prospective OLEDs

Wan M. Khairul [a,*], Anisatul Aqidah Tagiling [a], Ain Qarina Muzaman [a], Rafizah Rahamathullah [b,c], Mas Mohammed [a], Syaharil Saidin [a], Suhana Arshad [d], Ibrahim Abdul Razak [d], Fazira Ilyana Abdul Razak [e], Suhaila Sapari [e]

[a] Faculty of Science and Marine Environment, Universiti Malaysia Terengganu, 21030, Kuala Nerus, Terengganu, Malaysia
[b] Faculty of Chemical Engineering & Technology, Universiti Malaysia Perlis, 02600, Arau, Perlis, Malaysia
[c] Centre of Excellence for Biomass Utilization, Universiti Malaysia Perlis, 02600, Arau, Perlis, Malaysia
[d] X-ray Crystallography Unit, School of Physics, Universiti Sains Malaysia, 11800, USM, Penang, Malaysia
[e] Department of Chemistry, Faculty of Science, Universiti Teknologi Malaysia, 81310, UTM, Skudai, Johor, Malaysia

ARTICLE INFO

Keywords:
Chalcones
NLO active
Z-scan
Emissive layer
OLED

ABSTRACT

New derivatives of push-pull chalcone was successfully synthesized to demonstrate as NLO active on the impact of organic light emitting diode (OLED) materials. A total of three fused-aromatic chalcones (**AA, AB, AC**) with different substituents have been characterized through TGA, Z-scan analysis, ^{1}H & ^{13}C NMR, IR and UV–Vis. All the targeted compounds are nonlinear refraction (NLR) active with the range of $\chi(3)$ ($\sim \times 10^{-6}$ esu). **AC** reveals the highest value of first order hyperpolarizability (β_{tot}) at 528.08 $\times$ 10^{-30} esu upon the substitution of strong electron acceptor. Theoretical investigation was performed by employing the theory of B3LYP/6–31 G (d,p) level via density functional theory (DFT) to optimize the geometries, molecular electrostatic potential (MEP) and frontier molecular orbitals (FMO). The predicted electronic properties of the molecule are supported by the experimental results, confirming the theoretical conclusions. The examination of its potential as emissive layer in OLED application was constructed on ITO substrate for electroluminescence behaviour evaluation under various direct current (DC) voltages supply. The preliminary outcomes reveal that these simple chalcone derivatives are capable of being utilised in any optoelectronic application.

1. Introduction

At present, global research and development efforts are actively progressing in the technology sector to propel advancements in OLED displays, production techniques, layer architectures, organic materials and thin-film transistor backplanes[1-3]. In addition to addressing OLED's high cost and low-lifespan, various efforts are underway into the making of faster, more efficient and smaller electronic devices for everyday use[4-5]. Undoubtedly, conjugated organic compounds incorporating with the concept of Donor-Acceptor (D-A) substituent has become promising candidates in this area due to efficiency of charge transport, good emission and luminescent properties[6-7]. In fact, emissive compounds linked with multiple bonds and fused aromatic sytem namely pyrene[8], triphenylamine[9], antracene[10] unit have displayed good performance in OLEDs.

Chalcones and their derivatives have emerged as noteworthy contenders over the pass few years, therefore attracting attention for their electronic transport characteristics and making them preferred candidates among conjugated organic molecules for molecular devices [11-12]. Literally, chalcone derivatives have been explored as emitter and emissive layer in OLEDs due to the effect of aggregation-induced emission (AIE) and aggregation-induced emission enhancement (AIEE) [13-15]. Thus, precisely tuning the functional groups and substituents leads to good emission and luminescent properties. In this sense, research on electronic and optical properties of organic compounds has highlighted a plethora of luminescent research on fused aromatic chalcones[13,15-17]. Their conjugated structures, characterized by absolute delocalization in a π-electron system and two aromatic rings, render

* Corresponding author.
E-mail address: wmkhairul@umt.edu.my (W.M. Khairul).

https://doi.org/10.1016/j.molstruc.2024.139585
Received 12 May 2024; Received in revised form 22 July 2024; Accepted 5 August 2024
Available online 6 August 2024

them as promising candidates for luminescent studies and technological applications.

To date, highly fused aromatic chalcones stand out as exemplary derivatives within the chalcone family, showcasing a conjugated system with delocalized double bonds and π-electron structures across two aromatic rings. This conjugation imparts low redox potential, stability and exhibits visible light emission, making them appealing for future photonic and optoelectronic applications[9,11,18]. These derivatives are further distinguished by their noteworthy attributes of high blue-light transmittance and crystallizability, therefore gaining recognition for their potential in third-order NLO power limiting properties among organic materials. Chalcones, known for their diverse electronic properties, extend their utility beyond NLO materials to include applications as electrochemical sensors, optical limiters alongside their luminescent potential as OLEDs[19-21].

Additionally, substitution influences chromophores' photophysical properties by inducing shifts in absorption, steric effects and fluorescence, thus impacting fluorescence intensity based on electron mobility. Electron-donating substitution was found to enhance fluorescence, whereas electron-withdrawing ones decrease or eliminate it. Substitution also affects intersystem crossing and fluorescence quantum yield by factors such as molecular dipole moment and substitution position. Meanwhile, pyrene, a versatile fluorophore, is valued for its inertness, high fluorescence yield, and dual emission[8,11,13]. Interactions on Aggregation Induced Enhanced Emission (AIEE) with compact organic π-conjugated compounds will help exhibit intense emission[14]. Specific structural properties are crucial for chalcone derivatives to exhibit fluorescence, broadening their utility.

In this sense, computational chemistry using density functional theory (DFT) has become a more powerful tool to support experimental details[22-23] due to its great accuracy in reproducing the experimental values of molecular geometry, vibrational frequencies, atomic charges, dipole moment of a molecule's orbital interactions, as well as its structural and spectral characteristics[24]. By utilizing both computational and experimental analyses, this research aims to explore the potential of synthesized highly-fused aromatic chalcones as potential OLEDs materials.

2. Experimental and theoretical approach

2.1. Experimental assessments

2.1.1. Materials and instrumentations

The UV–Visible spectra in acetonitrile over the spectral range of 200–400 nm were recorded using Shimadzu UV–Vis 1800 Series Spectrophotometer. The recording was done in a 1 cm^3 cuvette, whilst the electronic emission spectra were documented within 200–900 nm using Varian Eclipse Fluorescence Spectrophotometer. The Bruker Avance III 400 Spectrometer (^{13}C: 100.61 MHz; ^{1}H: 400.11 MHz) is used for analysis with tetramethylsilane (TMS) as the internal standard and deuterated chloroform ($CDCl_3$) as a solvent. The analysis was conducted within the chemical shift ranges between δ_C 0–200 (^{13}C) and δ_H 0–15 ppm (^{1}H). In the spectral range of 4000–400 cm^{-1}, Invenio S Bruker Fourier Transform-Infrared Spectrophotometer was used to record vibrational infrared (IR) spectra. The spectra were obtained via the Platinum Attenuated Total Resonance (ATR) technique. Thermogravimetric analysis (TGA) was conducted on a Perkin Elmer TGA Analyzer, with a constant nitrogen gas flow, heating rate of 10 °C/min, and temperature range of 30 °C to 900 °C. Upon the preparation and product isolation of the derivatives (**AA, AB, AC**), the synthesized compounds were characterised spectroscopically and analytically. All solvents and chemicals were utilised as received from the standard commercial suppliers (Oxoid, Merck, Fisher Scientific, Acros Organics, Osilla, R & M Chemicals, Sigma Aldrich) without any additional purification before use in the experiment.

2.1.2. General synthetic approach

Preparation of highly fused aromatic chalcone derivatives (**AA, AB, AC**) started by adding 0.2 g of 1-pyren-1-ylethanone (0.82 mmol) into a two-necked round bottom flask containing 15 mL ethanol followed by non-stop stirring with a magnetic stirrer. Then, the designated benzaldehydes (**AA**: 4-(trifluoromethyl)benzaldehyde, **AB**: 4-ethoxybenzaldehyde, **AC**: 4-nitrobenzaldehyde) which was dissolved in 10 mL ethanol was added. The mixture was then left to become homogenous for a few minutes before 20 % sodium hydroxide was added dropwise and continuously stirred for *ca.*24 h. Thin layer chromatography (TLC) was utilized to monitor the reaction progress at suitable intervals, using a solvent system of hexane:dichloromethane (3:2). After determining the reaction completion through TLC, the mixture was carefully transferred to a beaker filled with ice cubes to cool down. The solution was then left undisturbed for the entire night, allowing the desired product to precipitate out of the solution gradually. The crude products were then filtered and dried over silica gel blue overnight. Lastly, the solid products formed in the reaction were purified through recrystallization from suitable solvents (**AA**: acetonitrile, **AB**: tetrahydrofuran, **AC**: ethyl acetate) until they turned into yellow crystalline solids. These solids were then filtered, dried and ready for further analysis and application. The process followed for synthesizing these solids is illustrated in Scheme 1.

2.1.2.1. (E-1-pyren-1-yl)−3-(4-(trifluoromethyl)phenyl)prop-2-en-1-one (AA). Yield 43 % (0.14 g) as yellow needle-like crystalline solids. m. p. 216.5 °C. **(ATR) FTIR cm^{-1}**: *ν*(C—H) aromatic 3050, *ν*(C=O) 1657, *ν*(C=C) 1601, *ν*(C-F) 1322. **^{1}H NMR (400.11 MHz, $CDCl_3$) ppm**: δ_H 7.56 (C═CH, d, $^{3}J_{HH}$ = 16 MHz, 1H); 7.67–7.73 (Ar-CH, m, 5H); 8.08–8.14 (Ar-CH, m, 2H); 8.20–8.26 (Ar-H, m, 3H); 8.28–8.31 (Ar-CH, m, 3H); 8.69 (C═CH, d, $^{3}J_{HH}$ = 9 MHz, 1H). **^{13}C NMR (100.61 MHz, $CDCl_3$) ppm**: δ_C 124.10 (C-F, s); 124.39, 124. 59, 124.97, 125.92, 125.96, 126.15, 126.33, 126.37, 126.52, 127.19, 128.57, 129.41, 129.50, 129.58, 130.65, 131.15, 133.16, 133.60 (Ar-CH, 18 x s); 133.60, 138.15 (C═CH, 2 x s); 195.14 (C=O, s). **EI-MS** *m/z*: Calcd. for $C_{26}H_{15}F_3O$ [M] 400.11; found 400.05 M^+. **Microelemental analysis for $C_{26}H_{15}F_3O$ [Theo. (Calc.)] %**: C [79.98 (77.93)], H [3.78 (3.69)].

2.1.2.2. (E-1-pyren-1-yl)−3-(4-ethoxyphenyl)prop-2-en-1-one (AB). Yield 82 % (0.25 g) as yellow crystalline solids. m. p. 218.6 °C. **(ATR) FTIR cm^{-1}**: *ν*(C—H) aromatic 3049, *ν*(C—H) alkyl 2986, *ν*(C=O) 1658, *ν*(C=C) 1583, *ν*(C—O) 1118. **^{1}H NMR (400.11 MHz, $CDCl_3$) ppm**: δ_H 1.45 (-CH_3, t, $^{3}J_{HH}$ = 7 MHz, 3H); 4.08 (-CH_2, q, 2H,); 6.92 (Ar-CH, pseudo-d, $^{3}J_{HH}$ = 9 MHz, 2H); 7.28–7.38 (C═CH, m, 1H); 7.53–7.63 (Ar-CH, m, 3H); 8.05–8.13 (Ar-CH, m, 2H); 8.19 (Ar-CH, d, $^{3}J_{HH}$ = 9 MHz, 2H); 8.24–8.27 (Ar-CH, m, 4H); 8.61 (C═CH, d, $^{3}J_{HH}$ = 9 MHz, 1H). **^{13}C NMR (100.61 MHz, $CDCl_3$) ppm**: δ_C 14.73 (s, CH_3); 63.68 (s, CH_2); 124.11, 124.50, 124.83, 124.92, 125.29, 125.88, 126.01, 126.08, 126.36, 127.20, 127.23, 128.93, 129.03, 129.26, 130.36, 130.74, 131.19, 133.04, 134.37 (19 x s, Ar-CH); 146.23, 161.28 (2 x s, C═CH); 196.29 (s, C=O). **EI-MS** *m/z*: Calcd. for $C_{27}H_{20}O_2$ [M] 376.15; found 376.00 $M^{+\cdot}$ **Microelemental analysis for $C_{27}H_{20}O_2$ [Theo. (Calc.)] %**: C [86.13 (76.33)], H [5.35 (4.60)].

2.1.2.3. (E-1-pyren-1-yl)−3-(4-nitrophenyl)prop-2-en-1-one (AC). Yield 54 % (0.17 g) as yellow cotton-like crystalline solids. m. p. 211.6 °C. **(ATR) FTIR cm^{-1}**: *ν*(C—H) 3057, *ν*(C=O) 1657, *ν*(C=C) 1590, *ν*(NO_2) 1319, 1279. **^{1}H NMR (400.11 MHz, $CDCl_3$) ppm**: δ_H 7.67–7.72 (Ar-CH, C═CH, m, 3H); 8.06–8.14 (Ar-CH, m, 2H); 8.10–8.25 (Ar-CH, m, 6H); 8.28–8.32 (Ar-CH, m, 3H); 8.72 (C═CH, d, 1H). **^{13}C NMR (100.61 MHz, $CDCl_3$) ppm**: δ_C 124.09, 124.16, 124.33, 124.50, 124.97, 126.26, 126.47, 126.59, 127.16, 128.92, 129.60, 129.69, 130.63, 131.12 (Ar-CH, 14 x s); 142.08, 148.54 (C═CH, 2 x s); 194.46 (C=O, s). **EI-MS** *m/z*: Calcd. for $C_{25}H_{15}NO_3$ [M] 377.11; found 377.00 M^+. **Microelemental analysis for $C_{25}H_{15}NO_3$ [Theo. (Calc.)] %**: C [79.55 (79.18)], H [4.01 (3.97)].

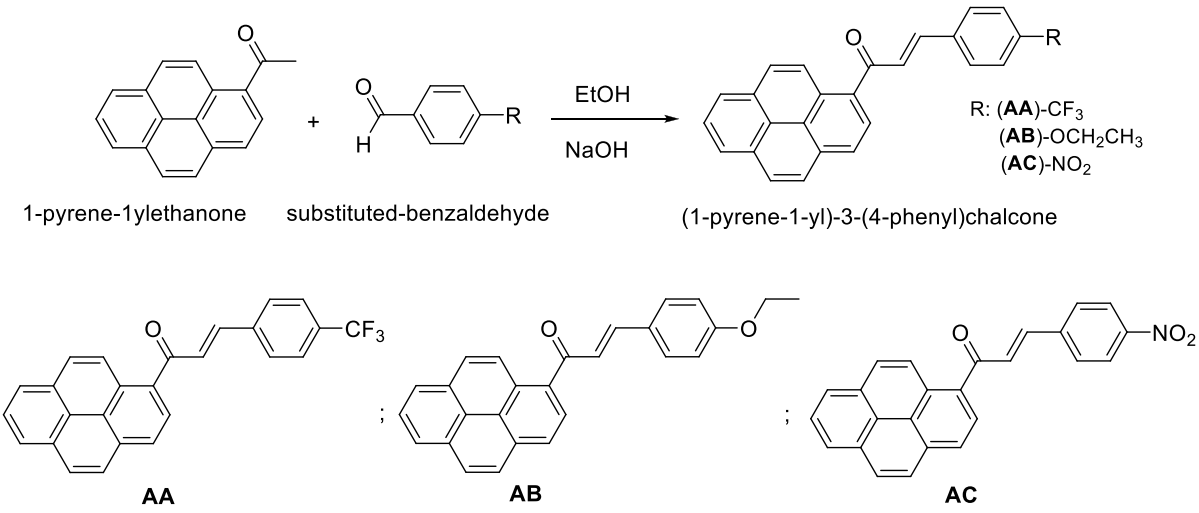

Scheme 1. General synthetic pathway of fused aromatic chalcone derivatives (**AA, AB, AC**).

2.1.3. Third order NLO: Z-scan measurement

The coefficients of the third-order NLO susceptibilities, namely the real and imaginary components (Re χ^3, Im χ^3), exhibit proportionality with respect to the NLR, n_2, and NLA coefficient (β). The DR201–95 KRUSS digital refractometer was used to measure the refractive index (n), whereas the absorbance of the UV–Vis spectra was used as a reference to evaluate the linear absorption coefficient (α). The single-beam Z-scan technique was used to determine the third-order NLO behaviour of **AA, AB**, and **AC**. This approach combines both nonlinear absorption (NLA) and nonlinear refraction (NLR), making it possible to measure them simultaneously. The measurements were carried out using a diode-pumped solid-state (DPSS) laser (Coherent Verdi-V5) operating at 532 nm in continuous-wave mode. The silicon amplified photodetector PDA55 was used as the detector. The quartz cuvette with a 1 mm path length was used to position the sample before analysis. The cuvette was then mounted on a LTS-300 precision motorized stage from Thorlabs. Table 1 tabulates the essential parameters for the Z-scan laser used in this study.

$\Delta T_{PV} = T_P - T_V$ referred to the transmittance between the peak and the valley. T_V and T_P are the normalized valley and peak transmittance, respectively. The difference between normalized peak-valley transmittance ΔT_{PV} is suggested by[25], whilst the difference in the normalized peak and valley transmittance (T_{PV}) was computed via Formula (1)[5-6].

$$\Delta T_{PV} = 0.406(1-S)^{0.25}|\Delta\varnothing_0| \tag{1}$$

The S denotes the linear transmittance of the aperture, while $|\Delta\varnothing_0|$ represents the phase shift that occurs at the focus along the optical axis (ω_a: laser spot radius before aperture; r_a: radius of aperture), which can be seen in Formula (2)[6].

$$S = 1 - \exp\left(-2r_a^2/\omega_a^2\right) \tag{2}$$

In the linear regime, ω_a represents the beam radium at the aperture.

Table 1
Z-scan laser parameters.

Parameters	Value
I_o	16.5 kW/ cm^2
S	0.42
Z_R	3.12 mm
λ	532 nm
w_o	23 μm
r_a	0.19 cm
f	20 cm

Nonlinear refractive index n_2 was quantified via the $\Delta\varnothing_0$ value in the relation $\Delta\varnothing_0 = kn_2I_0L_{eff}$, where $k = 2\pi/\lambda$ is the wave factor. Then, the nonlinear refractive index, n_2 is as Formula (3)[26].

$$n_2 = \frac{\Delta\varnothing_0\lambda}{2\pi I_0 L_{eff}} \tag{3}$$

$$T(Z) = 1 - \frac{4X\Delta\varnothing_0}{\left[\left(X^2+9\right)\left(X^2+1\right)\right]} \tag{4}$$

Where, $\Delta\varnothing_0$ is the nonlinear phase shift $X = Z/Z_0$, T(Z) is the normalized transmittance, Z_0 refers to the Rayleigh range and Z denotes distance of the cuvette[27]. Eq. (5) and Eq. (6) can be utilized to determine the real and imaginary components of the third-order NLO susceptibility[4,28]. The following equations refer to the speed of light as c, the vacuum permittivity as ε_0, and the linear refractive index of the compound as n_o.

$$Re\,\chi^{(3)}(esu) = \frac{10^{-4}\varepsilon_0 c^2 n_0^2 n_2}{\pi}\left(cm^2/W\right) \tag{5}$$

$$Im\,\chi^{(3)}(esu) = \frac{10^{-2}\varepsilon_0 c^2 n_0^2 \beta\lambda}{4\pi^2}(cm/W) \tag{6}$$

$$\chi^{(3)} = \sqrt{\left(Re\,\chi^{(3)}\right)^2 + \left(Im\,\chi^{(3)}\right)^2} \tag{7}$$

2.1.4. Electroluminescence analysis

Emissive layer of highly-fused aromatic chalcone derivatives (**AA, AB, AC**) were dip-coated in poly(3,4-ethylenedioxythiophene) polystyrene sulfonate (PEDOT:PSS), which was prepared beforehand on patterned indium-tin-oxide (ITO) thin films that acts as anode, whilst gold was used as the cathode. The layering arrangement of ITO-chalcone derivatives thin films is displayed in Fig. 1.

Concurrently, the current-voltage (IV) performance of these films was assessed using the Keithley 2400 Source Meter Unit (SMU) under ambient conditions, incrementally sourcing the voltage from 0 to 10 V at a step-size of 0.05 V using the KickStart software. Additionally, the electroluminescence properties were studied adopting the Twintex SP-3005 DC Power Supply in a dark environment, maintaining a constant current flow at a minimum of 5 V and gradually increasing the voltage (5 V – 30 V) to observe the escalation in light emission.

2.2. Theoretical assessments

Evaluation of the quantum-chemical data was performed computationally adopting the density functional theory (DFT) approach, using a

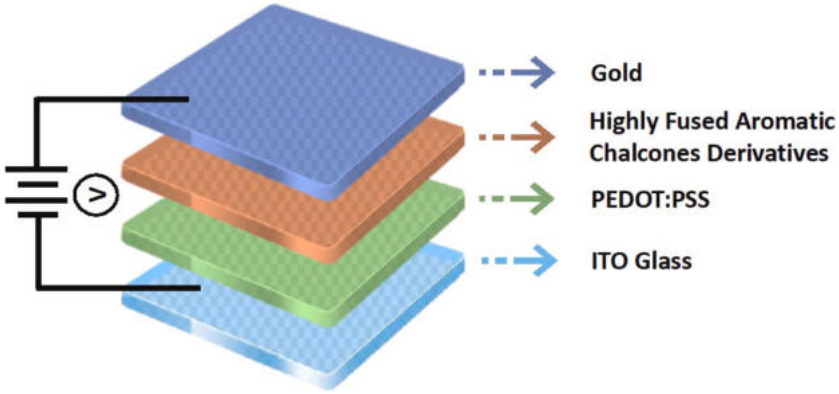

Fig. 1. The layering arrangement of ITO/chalcone derivatives thin films.

software package of Gaussian 09 W and GaussView 6.0. The calculations were based on a set of basis function at Becke-Style 3-Parameter using the Lee-Yang-Parr correlation functional (B3LYP) and 6–31 G (d,p). In addition, the reason for selecting the basis set was due to the fact that the results obtained using the B3LYP/6–31G(d,p) basis set exhibited considerably improved concurrence with the empirical observations. This includes the polarization function supplied, which yields more accurate bond lengths and a lower error[1]. Initial drawings in GaussView 6.0 were assessed using parameters outlined in Table 2. Besides standard FTIR and UV–Vis analyses, Gaussian 09 W was employed to generate and analyze optimized geometrical molecular electrostatic potential (MEP), frontier molecular orbital (FMO) and structural parameters energy maps for each fused-ring chalcone derivative.

Additionally, the computational NLO studies involved the calculation of first hyperpolarizabilities (β), dynamic linear polarizabilities (α) and electronic dipole moment (μ) to further investigate NLO properties of the molecule. The calculation for nonlinear optical (NLO) study was also conducted using the same program package, which was installed in the High-Performance Computing (HPC) facility at the Centre for Information and Communication Technology, Universiti Teknologi Malaysia, Skudai, Johor, Malaysia. The total dipole moment (μ_{tot}), anisotropic polarizability (Δα), isotropic polarizability (<α>), and total beta (β_{tot}) of the first-order hyperpolarizability and second-order hyperpolarizability (γ) were computed using the same method and basis set, as well as using established equations from previous studies [2-4].

$$\mu_{tot} = \left(\mu_x^2 + \mu_y^2 + \mu_z^2\right)^{1/2} \tag{8}$$

$$< \alpha > \frac{1}{3} = \left(\alpha_{xx} + \alpha_{yy} + \alpha_{zz}\right) \tag{9}$$

$$\Delta\alpha = \frac{1}{\sqrt{2}}\left[\left(\alpha_{xx} - \alpha_{yy}\right)^2 + \left(\alpha_{yy} - \alpha_{zz}\right)^2 + \left(\alpha_{zz} - \alpha_{xx}\right)^2 + 6\left(\alpha_{xy}^2 + \alpha_{xz}^2 + \alpha_{yz}^2\right)\right]^{1/2} \tag{10}$$

$$\beta_{tot} = \left[\left(\beta_{xxx} + \beta_{xyy} + \beta_{xzz}\right)^2 + \left(\beta_{yyy} + \beta_{yzz} + \beta_{yxx}\right)^2 + \left(\beta_{zzz} + \beta_{zxx} + \beta_{zyy}\right)^2\right]^{1/2} \tag{11}$$

Table 2
DFT parameters assessment using Gaussian 09 W.

Parameters	Method	Basis Set	Findings
Frequency	B3LYP, DFT, TD-SCF	6–31 G (d, p)	Vibrational Frequencies
Energy	B3LYP, DFT, TD-SCF	6–31 G (d, p)	UV–Vis, FMO, energy band gap, MEP
Optimization	B3LYP, DFT, Ground State	6–31 G (d, p)	Optimized and Stable Geometry

$$\beta_{tot=}\left(\beta_x^2 + \beta_y^2 + \beta_z^2\right)^{1/2} \tag{12}$$

3. Results & discussion

3.1. Molecular geometrical optimization

The synthesized optimized molecular structure of highly fused aromatic chalcone derivatives with its respective atom-numbering are shown Fig. 2. All derivatives share a common aromatic pyrene group with different substituents at the phenyl ring. The molecular design adheres to the D-π-A principle, where the aromatic pyrene group serves as the electron acceptor. In this study, the C27=C28 bond length of the chalcone aliphatic backbone for the chalcone derivatives are in the range of 1.34 – 1.35 Å, while the bond length for the C26=O37 are all approximately 1.23 Å. Additionally, the N42=O43 in **AC** bond length is also reported to have the same value of 1.23 Å. These bonds indeed revealed a double bond character, aligning closely within the expected values of 1.33 Å, with minimum deviations. However, the C–O bonds in **AB** (C36–O42, O42–C43) are slightly longer by 0.13 – 0.20 Å than the C=O, which may be attributed to the single bond characteristics of the carbonyl moiety. Moreover, the aliphatic backbone of chalcone connected to both sides (left and right) of the phenyl rings measures approximately 1.50 Å (C6–C26) and 1.46 Å (C28–C29), respectively. Meanwhile, the trifluoromethyl moiety in **AA** has a bond length of approximately 1.35 Å (C42–F45).

On the other hand, the bond angles for these derivatives at C=O bond of C6–C26=O37 and C27–C26=O37 are in the range of 121.79° – 122.65° and 119.82° – 120.90°, respectively. These approximately 120° angle centered at C26 within the chalcone moiety backbone implies that the carbons are sp2-hybridized[28-29]. This finding suggests a distortion in the compounds, which is visually represented by the twisted structure in Fig. 2. Meanwhile, the bond angles for C=C of C27=C28–C29 are at the range of 127.67° – 128.35°, respectively. The bond angles of phenyl rings are also approximately 118.55° – 121.76°. The bond at which the phenyl rings of the aliphatic backbone chalcones are connected, centering at C6, are approximately 118.44° – 119.00° Meanwhile, the bond centering at C43–O42–C36 in AB is measured at 119.08°.

Furthermore, the chalcone derivatives demonstrate significantly large torsion angles. The torsion angle centered at the C=C (H39–C27=C28–H38) is approximately 179.11° – 179.55°, in which **AA** and **AC** exhibiting clockwise rotations (bearing negative values). The torsion angles in which the aliphatic backbone of chalcone connected to the pyrene ring at C5=C6–C26=O37 for **AA** and **AC** is approximately 149.65° and 149.63°, respectively. Interestingly for **AB**, the torsion angle is at −31.64°. Additionally, the torsion angle at the right side connected to the substituents are in the range of 176.65° – 178.45°, with only **AB** rotating clockwise. Notably, the phenyl rings in the chalcone

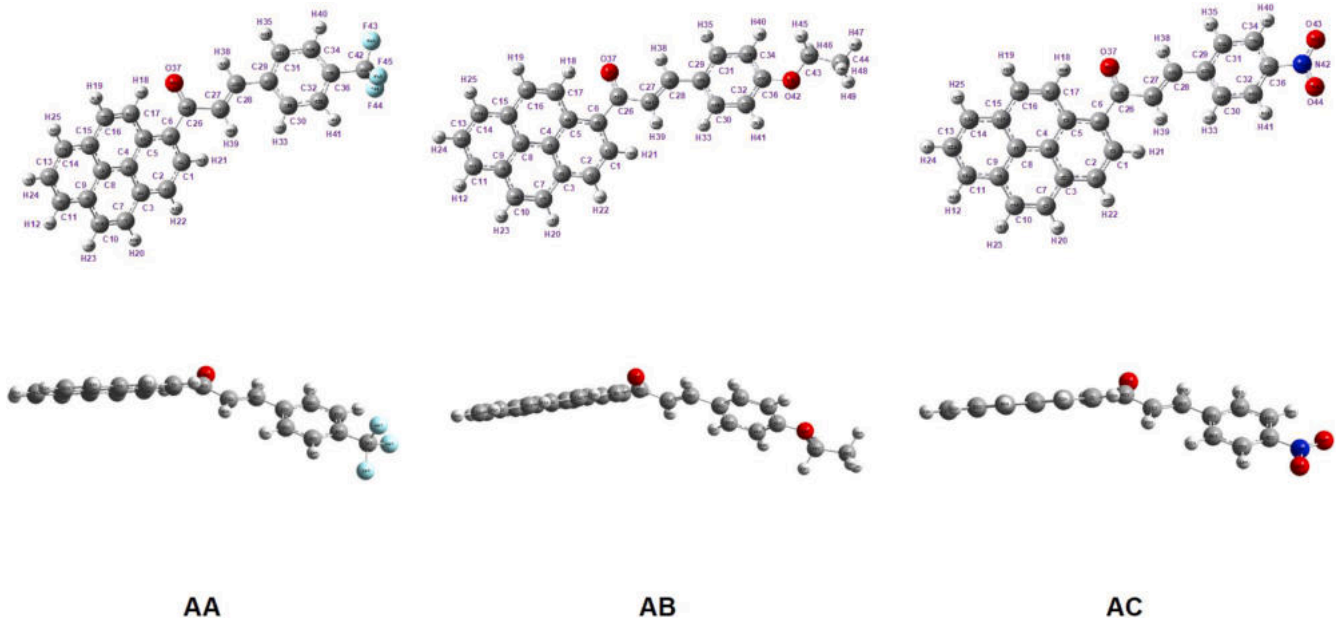

Fig. 2. Optimized molecular structure geometries of chalcone derivatives (**AA, AB, AC**).

derivatives all exhibit torsion angles of approximately 179° – 180°, indicating an anti-parallel and linear orientation, which has been visually in Fig. 2, particularly for the pyrene moiety. However, a slight deviation (distortion) from the perfect linearity in the molecular framework is observed at the bond C6–C26, as evidenced by the C5=C6–C26=O37 torsion angle values. Consequently, it can be inferred that the overall compounds of the chalcone derivatives in this study are non-planar. A comprehensive summary of the relevant parameters is provided in Table S1.

The considerable large dihedral angle between the bulky phenyl rings can significantly reduce the electronic effect in this context. Consistent with prior literature, the present theoretical computing finding indicates that all highly fused aromatic chalcone derivatives have non-rigid conformation and less planar geometry. The presence of bulky substituents, which causes intramolecular steric hindrance in polycyclic systems, is thought to be the key underlying reason causing these behaviors. Consequently, distortions among the phenyl rings are conceivable due to the inherent flexibility in conformation of the corresponding benzene fragments.

3.2. *Infrared vibrational frequencies (FTIR)*

The infrared (IR) spectra of the synthesized chalcone derivatives were investigated experimentally and theoretically to determine the functional groups and the spectra revealed three distinctive absorption bands namely – ν(C=C), ν(C=O) and ν(C—H). Both experimental and calculated IR spectra in this current work correlated to each other and they reveal all of the expected vibrational frequency regions, which is reported in Table 3, whilst the spectra are depicted in Figs. S1 and S2. The calculations were made for free molecules in vacuum, which means that the theoretical values are higher than the values obtained from experiments that were conducted on crystalline solid samples. Additionally, due to the combination of basis set limitations and electron correlation effects, computed frequencies were often greater than comparable experimental numbers[30]. The wavenumbers that were not scaled were multiplied with a uniform scaling factor of 0.967 to ensure that they matched the experimental results[31-32].

The absorption bands corresponding to ν(C—H) aromatic group of the chalcone derivatives were observed in the range of 3049–3057 cm^{-1} with medium intensity, aligning with the typical range (3010–3100 cm^{-1}) of C—H stretching vibrations[32]. Theoretically, C—H stretching wavenumber can be observed at the range of 3084–3204 cm^{-1}. This finding is consistent with a previous study reported that the wavenumber for aromatic C—H stretching can be found at the range of 3100–3000 cm^{-1}, with its significance in the spectrum of benzene derivatives making it especially evident[33]. The theoretically computed

Table 3
Absorption data for designated chalcone derivatives (AA, AB, AC).

Compound	Vibrational Assignment	Experimental FTIR	Calculated FTIR [B3LYP/6–31 G (d,p)]		Percentage Deviation (%)
		Frequency (cm^{-1})	Frequency (cm^{-1})	Scaled Frequency	
AA	ν(C–H) aromatic	3050	3334	3204	5.0
AB		3049	3334	3204	5.1
AC		3057	3209	3084	0.9
AA	ν(C=O)	1657	1727	1660	0.2
AB		1658	1711	1644	0.8
AC		1657	1736	1668	0.7
AA	ν(C=C)	1601	1686	1620	1.2
AB		1583	1677	1612	1.8
AC		1590	1661	1596	0.4
AA	ν(C-F)	1271, 1322	1369	1316	0.5, 3.5
AB	ν(C–H)	2986	3267	3140	5.2
	ν(C–O)	1118	1253	1204	7.7
AC	$\nu(NO_2)$	1279, 1319	1386, 1394	1332, 1340	1.6, 4.1

scaled-down vibrations corresponding to *ν*(C—H) aromatic stretch within this study exhibited close agreement with the experimentally measured vibrations with 0.9–5.2 % of percentage deviation. Additionally, the C–H stretching of alkyl groups in **AB**, attached to the oxygen atom can be observed at approximately 2986 cm^{-1}, falling within the range of 2849 – 2922 cm^{-1} as reported previously[34].

The ν(C=O) absorption band in the chalcone derivatives was anticipated around 1657–1658 cm^{-1} (experimental) and 1660–1668 cm^{-1} (theoretically), falling within the expected range (1660 – 1710 cm^{-1}), attributed to the resonance effect of the carbonyl group with the phenyl ring and intermolecular hydrogen bonding in the molecules[35-36]. The effect of π-electron delocalization between β and α carbons results in increased bond order between the a carbon atom and carbonyl and decreased C=O order, may also explain the detection to the lower wavenumber C=O. Disparities in the range are also mainly influenced by bond strength, dictated by steric effects, conjugative, inductive and lone pair of electrons on oxygen[3,33]. For **AB**, a strong stretching band of *ν*(C—O) is observed at 1118 cm^{-1} (experimental) and 1204 cm^{-1} (theoretical), a range associated with intermolecular hydrogen bonding in the molecule. Additionally, *ν*(C=C) is detected around 1600 cm^{-1} when conjugated with *ν*(C=O) group.

Due to varied substituents among compounds, distinct vibrational variations were observed. The ν(C-F) stretching vibrations are noted at roughly 1271–1322 cm^{-1} (experimental) and 1316 (theoretical) in **AA**, whilst the vibrations at 1114 cm^{-1} and 2981 cm^{-1} are attributed to alkyl groups and ν(C—O) bonds connected to the aromatic ring in **AB**. Lastly, the nitro group in **AC** contributes to the region of 1279 – 1319 cm^{-1} (experimental) and 1332–1340 cm^{-1} (theoretical), indicating asymmetric stretching vibrations of the NO_2 group. The study discovered that the percentage deviation among DFT and experimental calculations was within 0.2–7.7 %.

3.3. ^{1}H & ^{13}C nuclear magnetic resonance (NMR)

The structure of fused aromatic chalcones (**AA, AB, AC**) were identified and validated using both analyses of ^{1}H and ^{13}C Nuclear Magnetic Resonance (NMR) spectra. Residual peaks pertaining to solvent and impurities were also observed in all spectra. Resonances for the solvent and internal standard, deuterated chloroform ($CDCl_3$) and tetramethylsilane (TMS), were observed at δ_H 7.28 ppm and δ_H 0.04–0.12 ppm, respectively. The ^{1}H NMR spectra showed distinctive unresolved overlapping signal of aromatic protons that can be observed at δ_H 6.94–8.32 ppm as pseudo-doublet and multiplet, which is aligned with literature [37]. Additionally, the alkene moieties were observed at δ_H 7.38–8.73 ppm where, **AA** were identified at δ_H 7.58 and 8.70 ppm (*J*-coupling:16 MHz and 9 MHz, respectively) while **AB** were observed at δ_H 7.38 and 8.62 ppm (*J*-coupling: 13 MHz and 9 MHz, respectively). The alkene moieties of **AC** were found at δ_H 7.61 and 8.73 ppm (*J*-coupling: 16 MHz) as doublet resonance multiplet due to the overlapping between aromatic and doublet resonance which indicates the *E*-configuration of synthesized chalcone. According to previous literature, the strong value of coupling constant indicates the confirming of *trans*-conformation of the C=C bond[29].

Furthermore, the ^{13}C NMR spectra revealed two vinylic resonances for each compound (**AA**: δ_C 138.15 ppm and 143.55 ppm; **AB**: 146.23 ppm and 161.28 ppm; **AC**: 142.08 and 148. 54 ppm), in which referring to the splitting of *α* and *β* unsaturated carbons, respectively, due to unsymmetrical nature of the molecular framework. The aromatic carbons were identified in the range of δ_C 124.09 to 134.37 ppm, with carbon in Ar-benzene having the largest chemical shift due to its location next to the electronegative N atoms. In addition, the chemical shift of $–CH_3$ of **AB** was expected at δ_C 14.73 ppm due to the deshielded effect in the presence of an oxygen atom that withdraws certain amount of electron density from the alkyl chain. Moreover, the $–CH_2$ was allocated at δ_C 63.68 ppm. The C=O resonances of **AA–AC** were found as singlet resonances at δ_C 194.46 to 196.29 ppm due to the deshielding effect which affected the chemical shift according to the presence of nearby oxygen atom. Both ^{1}H and ^{13}C NMR of titled chalcone derivatives spectra can be observed in Figs. S3–S8. Whereas, Table S2 and S3 tabulate the summarized chemical shift of both ^{1}H and ^{13}C NMR analysis of the synthesized compounds.

3.4. Ultraviolet electronic absorption and optical analyses

The Beer-Lambert Law is typically utilized to quantitatively assess the structure of organic compounds by analyzing their maximum wavelength. Experimental and theoretical spectra of highly-fused aromatic chalcone derivatives is shown in Fig. 3. The electronic spectra for fused aromatic chalcone derivatives were recorded in dichloromethane (10^{-5} M) with a cut-off solvent residue of 230 nm.

The UV–Vis spectra revealed two prominent electronic transitions: π → π* and n → π*. The shorter wavelength region around 242 – 243 nm was assigned to the π → π* transition, attributed to the overlapping of phenyl rings and carbonyl (C=O) moieties. Various substituents on the phenyl rings induced bathochromic (red) shifts, with stronger electron-donating groups affecting the π → π* transition and lower FMO energy band gap[32]. Moreover, presence of pyrene in the system causes extended conjugation, thus contributing to this red shift. There are also two visible absorptions that can be seen at 277 nm (**AC**) and 293 nm (**AA**), which may be attributed to the carbonyl group. Additionally, it could also be seen that the phenyl rings, C=O and C=C groups contributed to n → π* transitions that can be observed in the 325 – 409 nm region. The summarized data can be observed in Table S4.

In comparison to the computed optical spectra, each compound exhibited one major absorption (**AA**: 448 nm, **AB**: 405 nm, **AC**: 517 nm). The region revealed a mix transition of π → π* and n → π*, which may be attributed to the excitation from HOMO to LUMO with the presence of aromatic rings, C=O and C=C moieties. The differences in absorption wavelengths were attributed to variations in the electronegativity values of the substituents (**AC**: –NO > **AA**: $–CF_3$ > **AB**: $–OCH_2CH_3$).

Meanwhile, the absorption and fluorescence emission spectra were measured in dichloromethane (1×10^{-5} M), revealing an interesting relationship: the UV-F emission spectra closely mirrored their respective absorption spectra, a phenomenon known as the Stokes shift. Notably, molecules become intriguing candidates for display device applications when the Stokes shift exceeds 95 nm, indicating higher excitation energies than emission energies[38]. It was postulated that compounds exhibiting significant Stokes shifts held promise as fluorescent materials for OLEDs, underscoring the potential impact of these findings on optoelectronics development and applications.

Among all three derivatives, only **AB** displayed pronounced UV-F, while **AA** and **AC** exhibited minimal intensity. The UV-F spectrum of **AB**, depicted in Fig. 4, showcased a strong Stokes shift of 89 nm, derived from emission and absorption wavelengths of 344.84 nm and 433.93 nm, respectively. Conversely, the UV-F spectrum of all derivatives has been depected in Fig. 5 and the lack of fluorescence in **AA** and **AC** was attributed to the steric hindrance within the molecular framework, which reduces quantum yield. This hindrance may stem from substituents attached to chalcone derivatives, particularly electron-withdrawing groups present in **AA** and **AC**. Additionally, the low emission quantum yields could result from the electronic push-pull action within the molecules, influencing intramolecular charge transfer and hydrogen bonding dynamics[37].

3.5. FMO and energy band gap

Frontier Molecular Orbital (FMO) theory stands as a fundamental tool for both electrical and optical analyses, employing molecular orbitals – specifically, the Lowest Unoccupied Molecular Orbital (LUMO) and Highest Occupied Molecular Orbital (HOMO) to anticipate reactive sites in conjugated systems. The HOMO serves as an electron donor due to its ionization potential, whilst LUMO accepts electrons and its energy

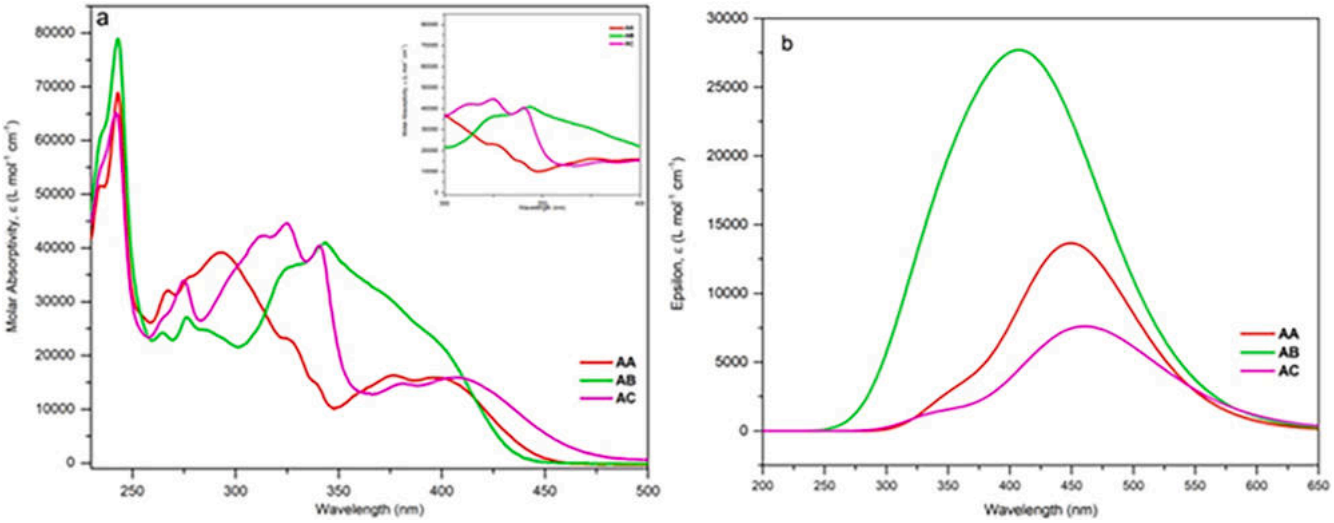

Fig 3. (a) Experiment (b) theoretical UV–Vis spectra of chalcone derivatives (**AA, AB, AC**).

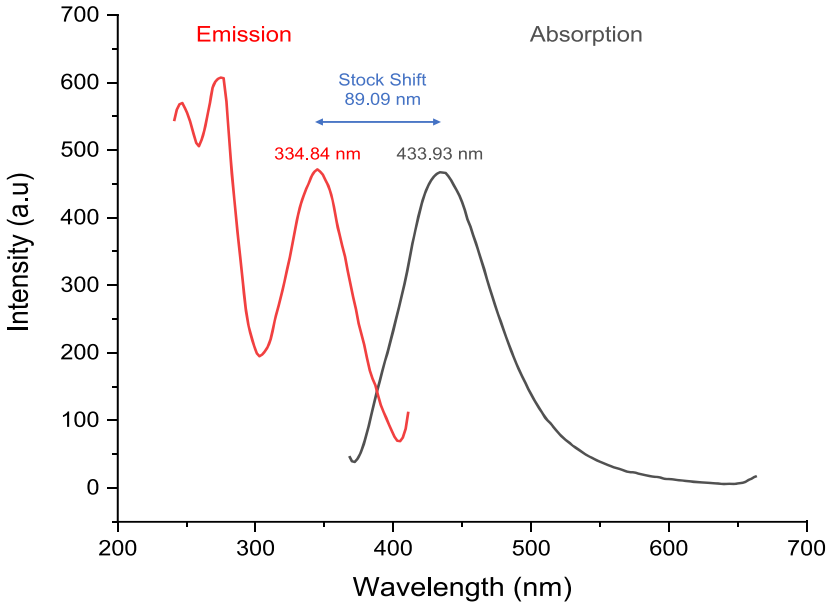

Fig. 4. The UV-fluorescence spectrum of **AB** recorded in dichloromethane.

is linked to electron affinity[39]. A smaller FMO gap is an indicative of heightened polarizability and increased chemical reactivity, but diminished kinetic stability. The HOMO-LUMO energy band gap assigned the molecular chemical stability which was utilized to ascertain the electrical transport in molecular framework. Fig. 6 provides a visual representation of the HOMO and LUMO for each compound under scrutiny.

The transfer of electron density happens within the π-conjugated system on the electron-donor side, from the more aromatic portion towards its electron-withdrawing part. Fig. 6 reveals that the π nature of the HOMO is delocalized across the pyrene and C=O moieties. Interestingly, the LUMO was distributed throughout the molecule except for **AC**, which only covers the left side of the compound. This finding may be attributed to the push-pull effect in **AC**, which might cause a partial coverage of the LUMO due to asymmetric electron redistribution. Nonetheless, these contours confirm the system undergoes electronic transitions. It becomes apparent that the chalcone group primarily functions as an electron acceptor due to its shape in the LUMO region. However, it is deficient in the HOMO region where it fails to be an electron donor. It is shown that **AC** has the smallest FMO energy gap of 2.71 eV compared to **AB** and **AA**, with the energy separations of 3.29 eV and 3.09 eV, respectively. The lower value of energy band gap contributed to the high reactivity, chemical stability and ability of the molecule to transfer larger number of electrons through π-conjugation from HOMO to excited stated LUMO within molecules lead to the high value NLO properties[25].

The energy band values of these compounds had shown their potentiality as semiconducting materials as we can expected to differ due to the differences of substituents attach to the chalcone moieties that small HOMO–LUMO separation characterizes conjugated molecules, which is the consequence of intramolecular charge transfer from the end-capping electron-donor groups to the efficient electron-acceptor group through the π-conjugated route[40]. Thus, one can conclude that the energy band values of all these compounds are indeed having semiconductor properties. Table 4 shows the major involvement of the electronic excitation energies from ground state (S_0) to the excited state

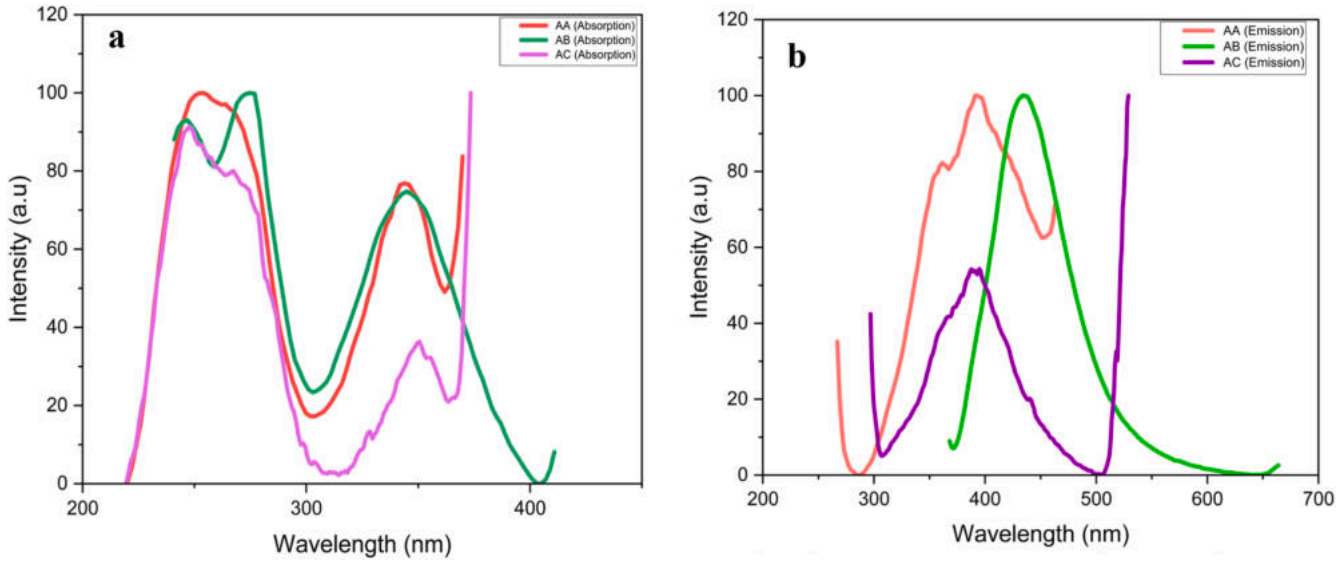

Fig. 5. (a) Absorption spectra and (b) Emission spectra of **AA, AB** and **AC** recorded in dichloromethane.

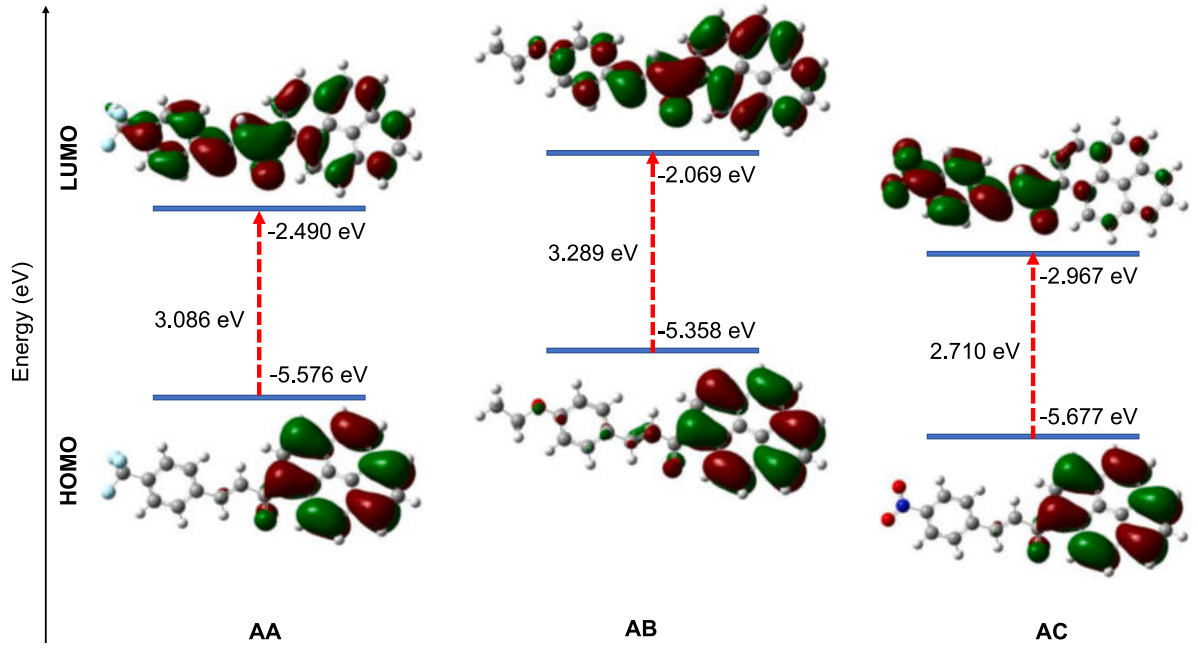

Fig. 6. FMO energy gap of synthesized chalcone derivatives (**AA, AB, AC**).

Table 4
Significant FMO parameters.

Compound	Wavelength, (nm)	Excitation energy (eV)	Oscillator Strength (f_o)	Assignments, major contributors (%)
AA	451	2.75	0.33	$S_0 \rightarrow S_n$ (69.49 %)
AB	419	2.96	0.57	$S_0 \rightarrow S_n$ (68.57 %)
AC	519	2.39	0.17	$S_0 \rightarrow S_n$ (70.41 %)

(S_n) of these compounds.

3.6. Global chemical reaction descriptors (GCRDs)

Electronic chemical potential (μ) and chemical hardness (η) are determined from EA and IP, whilst reactivity descriptors such as electron affinity (EA) and ionization potential (IP) are assessed from HOMO and LUMO. According to Koopman's theorem, it is possible to draw the conclusion that the HOMO and LUMO orbital energies of a compound are indicative of both its EA and IP. The equations given below are used to approximate the formula of each GCRDs, while summarized data is tabulated in Table 5:

$$IonizationPotential, IP = -E_{HOMO} \quad (13)$$

$$ElectronAffinity, EA = -E_{LUMO} \quad (14)$$

Table 5
GCRDs theoretical data of highly fused aromatic chalcone derivatives.

Parameter (eV)	AA	AB	AC
E_{HOMO}	–5.576	–5.358	–5.677
E_{LUMO}	–2.490	–2.069	–2.967
Energy Gap	3.086	3.289	2.710
Ionization Potential, IP	5.576	5.358	5.677
Electron Affinity, EA	2.490	2.069	2.967
Electronegativity, χ	4.033	3.714	4.322
Chemical Potential, μ	–4.033	–3.714	–4.322
Chemical Softness, S	0.648	0.608	0.738
Chemical Hardness, η	1.543	1.645	1.355
Electrophilicity Index, ω	5.271	4.193	6.893
Electron Donating Ability, ω^-	7.480	6.255	9.223
Electron Accepting Ability, ω^+	3.447	2.542	4.901

$$Electronegativity, \chi = (IP + EA)/2 \quad (15)$$

$$ChemicalHardness, \eta = (IP - EA)/2 \quad (16)$$

$$Softness, S = 1/\eta \quad (17)$$

$$Chemical\ Potential, \mu = -(IP + EA)/2 \quad (18)$$

$$Electrophilicity\ Index, \omega = \mu^2/2\eta \quad (19)$$

$$Electron\ Donating\ Ability, \omega^- = (3IP + EA)^2 \Big/ 16(IP - EA) \quad (20)$$

$$Electron\ Accepting\ Ability,\ \omega^+ = (IP + 3EA)^2 \Big/ 16(IP - EA) \quad (21)$$

During molecular interactions, the LUMO corresponds to the EA, which absorbs electrons as well as its energy. Moreover, the IP of a molecule is represented by the HOMO, which corresponds to electron donors. From the presented calculations, it is apparent that **AC** has the highest EA while **AB** demonstrates the lowest value for both IP and EA. Electronegativity, as proposed by Pauling, describes the ability of an atom within a molecule to attract electrons towards itself, thereby influencing electrophilicity—the molecule's propensity to accept electrons. Among the synthesized compounds, electronegativity follows the order of **AB** (3.71 eV) < **AA** (4.03 eV) < **AC** (4.32 eV), which aligns with the nature of the substituents bonded to the benzene of the chalcone moiety.

Furthermore, the stability and reactivity of a chemical system are determined by the chemical hardness of a compound. Chemical hardness quantifies the resistance to changes of the molecules in charge transfer or electron distribution. On the basis of FMO, this descriptor corresponds to the gap between the HOMO and LUMO, which led to the conclusion that the harder the molecule, the less reactive and more stable it is. With **AB** showing the optimum hardness value at approximately 1.65 eV, indicating the largest FMO energy gap, it can be suggested that it possesses the highest stability. Findings have demonstrated that **AB** has the lowest hardness level among the three, whereas the hardness level of **AA** is intermediate between that of **AB** and **AC**. Conversely, the chemical hardness and chemical potential (μ) are inversely related. The chemical hardness is used to determine the tendency of electrons to escape from a system at equilibrium. It has also been supported that chemical potentials with higher values are more reactive than those with lower electronic chemical potentials.

Lastly, the global electrophilicity index (ω) gauges the energy stabilization of a system upon receiving additional electronic charges and measures its capacity to accept electrons. Based on thermodynamic principles, Parr *et al.* were the first to develop a method for assessing the increase in energy that occurs when a chemical system achieves saturation through the introduction of electrons. It is computed via the chemical hardness and electronic chemical potential, which is shown in the list of equations.

3.7. Molecular electrostatic potential (MEP)

The Molecular Electrostatic Potential (MEP) offers insights into the net electrostatic effect generated by a molecule's total charge distribution, providing information on chemical reactivity, partial charges, electronegativity and dipole moments. Visualized through an electron density isosurface mapped with electrostatic potential surface, MEP offers a tangible representation of a molecule's relative polarity[41], as depicted in Fig. 7.

As can be observed, distinct colors in the MEP map signify varying electrostatic potential values: red indicating the most electronegative potential (strongest aversion), blue representing the most positive potential (strongest aversion), and green indicating zero potential. MEP rises in the following order: red < orange < yellow < green < blue. The study reveals that **AA, AB** and **AC** have different MEP scales, ranging from −4.804 a.u. (deepest red) to +4.804 a.u. (deepest blue), −5.640 a.u. to +5.640 a.u. and −4.621 a.u. to +4.621 a.u., respectively. The lone pair of electronegative atoms is frequently connected with negative potential regions. Electronegative oxygen atoms of the alkoxy and nitro groups predominantly exhibit negative potential zones, serving as possible sites for electrophilic attack, whilst the hydrogen of phenyl rings corresponds to nucleophilic positive regions. Therefore, this comprehensive MEP analysis unveils the distinct electrostatic characteristics of each compound.

3.8. Thermal behavior and stability

Thermogravimetric analysis (TGA) serves as a crucial method for evaluating the kinetic and thermodynamic properties of substances, revealing thermal stability and weight loss. Material stability during fabrication is paramount in OLED production, necessitating long-term resilience in high-temperature environments for sustained performance. Fig. 8 reveals two stages of degradation process of the fused aromatic chalcone derivatives, while Fig. 9 depicts the overlaid thermogram of thermogravimetric (TG) and differential thermogravimetric (DTG).

All three compounds mentioned were subjected to detailed characterization and analysis of their corresponding behaviors and thermal stabilities adopting a thermogravimetric analyzer, aligning with the requisite evaluation for developing high-temperature-resistant OLED thin films at more than 200 °C[42]. Results indicated stability up to approximately 200 °C with two distinct mass loss in the degradation processes. Notably, no weight loss was reported at 100 °C, indicating the absence of water molecules in the samples. The summarized thermal analysis in Table 6 reveals that higher temperatures are required for mass loss, attributed to larger molecular weight and a rigid conjugated bonding system.

The first degradation occurs between 240 °C – 490 °C, while the second degradation process unfolds at around 400 °C – 880 °C, with substantial weight loss of more than 50 % (**AA**: 55 %; **AB**: 76 %; **AC**: 68 %). From these numbers, it is derived that **AB** exhibits the highest onset temperature for both the first and second degradation steps, indicating greater thermal stability in compared to **AA** and **AC**. This may be attributed to the fact that **AB** has a D-π-D system in comparison to **AA** and **AC**, which consisted of D-π-A system due to the nature of substituents affecting the thermal stability of the compounds. However, **AA** shows the lowest weight loss percentage during degradation, suggesting relatively higher resistance to thermal decomposition. Compound **AC** falls between **AA** and **AB** in terms of both onset temperatures and weight loss percentage. The first degradation likely involves the decomposition of volatile components, leaving behind residual carbon mass (**AA**: 32 %; **AB**: 24 %; **AC**: 46 %). Additionally, the attachment of substituent with high molecular weight decreases its thermal stabilities towards extreme temperature[43]. Hence, these findings underscore the compounds' potential suitability in OLED fabrication due to their stability to withstand extreme temperatures.

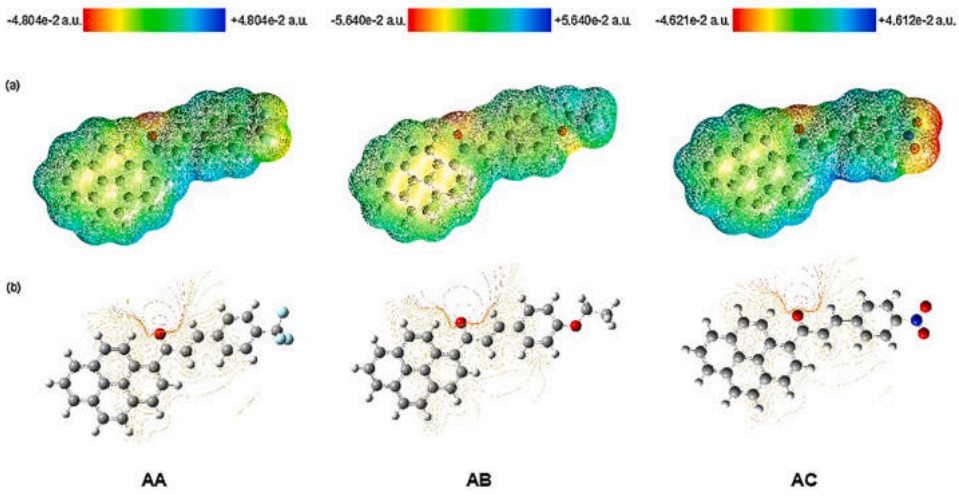

Fig. 7. MEP of highly fused aromatic chalcone derivatives (**AA, AB, AC**).

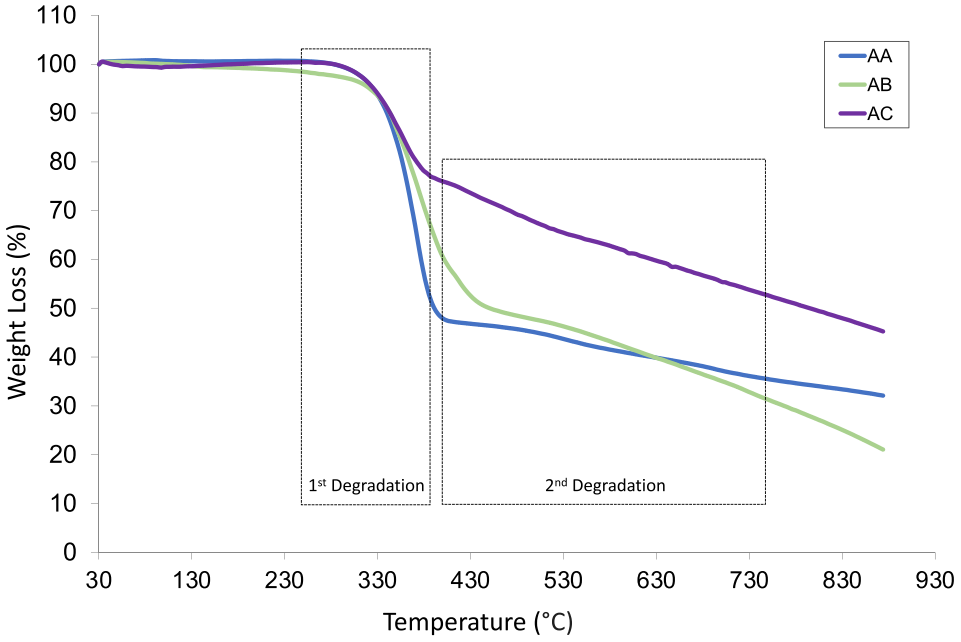

Fig. 8. TGA thermogram of fused aromatic chalcone derivatives (**AA, AB, AC**).

3.9. Experimental and theoretical studies of 3rd order NLO

3.9.1. NLO computational calculations

Nonlinear optical (NLO) studies how the interaction of applied electromagnetic fields to produce new electromagnetic field changed in amplitude, frequency, phase and other physical properties. The computational calculation was conducted to evaluate the NLO properties such as hyperpolarizabilities (β), polarizability (α) and dipole moment (μ). Compounds with considerable NLO properties usually have push-pull conjugated structure, with π- electron conjugated moiety substituted by an electron donor group an electron acceptor group on the ends[44-45]. Table 7 tabulates the associated parameters that were obtained.

The computed total static dipole moments for **AA, AB** and **AC** are 3.20, 4.69, and 5.61, respectively, which surpassed previous reported values[46]. The highest dipole moment of **AC** due to the strong donor-acceptor configuration of the compound. Notably, these values exceed the standard urea dipole moment of 1.37. Both the computed static anisotropic polarizability (Δα) and static isotropic polarizability (<α>) of the titled chalcones fall in the order of 10^{-24} esu, indicating heightened polarization attributed to the increased dipole moment. Furthermore, the first polarizability β_{tot} stands at a favorable range [β_{tot} ($\times$ 10^{-30} esu) – **AA**: 201.55; **AB**: 101.44, **AC**: 528.08], which are larger than the previous reported study[45]. **AC** shows a significantly higher value of β_{tot} than **AA** and **AB** due to the intramolecular charge transfer in the molecular framework from donor group to acceptor group. These exceptional NLO properties can be ascribed to their large dipole moment, polarizability and small energy band gap, thus placing them within the range of organic semiconductor materials for ideal NLO device applications.

3.9.2. Z-scan measurement

The Z-scan measurements of titled fused aromatic chalcones at a wavelength of 532 nm are presented in Fig. 10, showcasing both closed aperture (CA) and open aperture (OA) curves. The focal point, where the OA normalized transmittance curve reaches a minimum, signifies

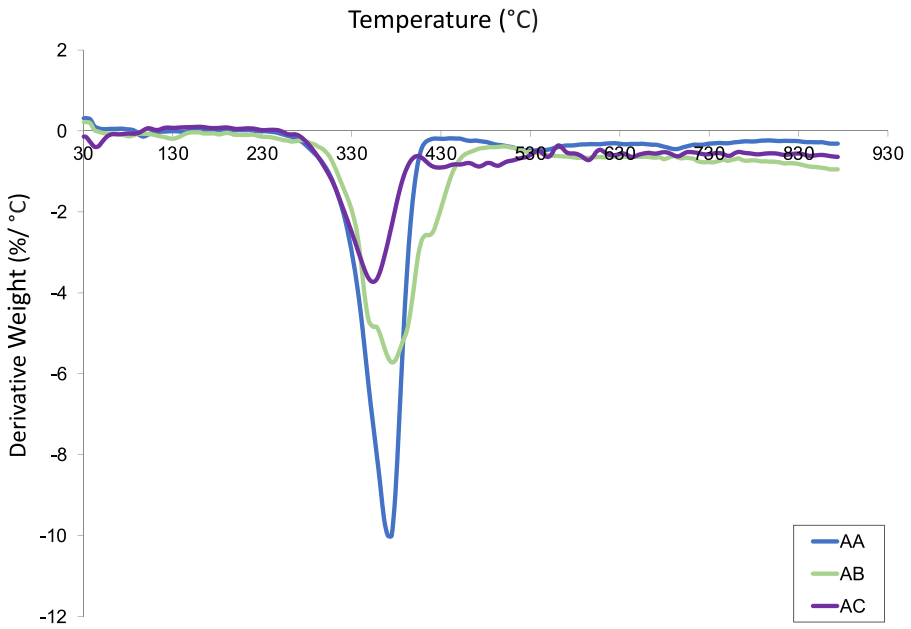

Fig. 9. Differential thermogravimetric (DTG) curves of fused aromatic chalcone derivatives (**AA, AB, AC**).

Table 6
Thermal analyses of fused aromatic chalcones (**AA, AB, AC**).

Compound	Degradation Step	Onset Temperature, T_{onset} (°C)	Offset Temperature, T_{offset} (°C)	Weight Loss (%)
AA	First	241.30	425.91	68.00
	Second	455.61	873.79	
AB	First	271.38	484.90	76.03
	Second	506.21	873.88	
AC	First	267.40	400.52	54.51
	Second	409.01	873.29	

Table 7
Value of 1st order hyperpolarizability, polarizability and dipole moment.

NLO Parameters	AA	AB	AC
Dipole moment (Debye)			
μ_{tot}	3.20	4.69	5.61
Polarizability, α ($\times$ 10^{-24} esu)			
α_{xx}	51.95	56.23	18.02
α_{yy}	42.87	45.05	46.06
α_{zz}	17.70	19.73	99.93
α_{xy}	−0.31	1.53	−6.26
α_{xz}	6.78	−5.86	0.49
α_{yz}	−0.19	−1.21	−14.53
$< \alpha >$	51.95	56.23	54.67
Δα	69.54	75.56	77.14
1st Hyperpolarizability, β ($\times$ 10^{-30} esu)			
β_{xxx}	1.23	12.85	−0.15
β_{xyy}	−0.69	−0.33	−0.37
β_{xzz}	−15.27	−18.52	−4.51
β_{yyy}	1.37	0.68	1.84
β_{yxx}	−0.21	−2.24	0.22
β_{yzz}	14.51	9.15	22.45
β_{zzz}	−57.79	−16.98	−168.74
β_{zxx}	−2.23	−12.66	−0.93
β_{yyz}	−3.73	−3.22	−4.59
β_{x}	−44.01	−18.28	−11.75
β_{y}	49.29	23.85	75.82
β_{z}	−190.41	−96.89	−522.48
β_{tot}	201.55	101.44	528.08

reverse saturable absorption in both chalcones. The OA curve (Fig. 10a) facilitates the calculation of nonlinear absorption (NLA) for the titled compounds that exhibits positive β coefficients. The curve's pattern reveals strong reverse saturable absorption (RSA), a characteristic of NLO materials marked by greater excited state absorption than ground state absorption. Notably, the pyrene moiety's electrons, acting as a donor group with strong intramolecular transfer (ICT), contribute significantly to RSA[28]. The π-conjugated system enables charge transfer through these molecular frameworks, thereby augmenting the activity of NLO. The NLO spectrum of the CA (Fig. 10b) illustrates the peak and valley profiles indicative of nonlinear refraction, n2 (cm^2/W), which can be seen for the synthesized compounds as 3.37×10^{-11} (**AA**), 8.80×10^{-11} (**AB**) and 3.40×10^{-11} (**AC**), respectively. Table 8 summarizes the β and n2 values obtained through nonlinear fitting using the Levenberg-Marquardt algorithm, as depicted by the red lines in Fig. 10. The magnitude of NLO susceptibility, $\chi^{(3)}$ ($\times$ 10^{-6} esu) [**AA**: 0.15; **AB**: 9.74 **AC**: 0.13], exceeds that of other reported chalcone derivatives[25, 28,46]. Several factors, including intermolecular interactions, planarity, conjugation length and ICT, can affect the NLO properties of these compounds[47]. These greater $\chi^{(3)}$ values indicate efficient electron density transfer throughout the molecular framework system which are influenced by the electron donating-accepting groups' abilities.

3.10. Electroluminescence properties

The fabrication of OLED thin films followed the device structure: ITO/PEDOT:PSS/chalcone derivatives (**AA, AB, AC**)/Gold. These prototypes then were connected with conducting wire as a complete circuit to measure their conductivity and electroluminescence behavior. Current-Voltage (IV) curve analysis, depicted in Fig. 11, illustrates a direct correlation between voltage (V) increase and current (I) increment in the range of −5 V to 5 V, indicative of charge transfer from the N-doped group (positive charge donor) to the P-doped group (negative charge acceptor) within the highly fused aromatic chalcone derivatives, resulting in recombination and the P-N junction formation, which pertains to semiconductor properties[48]. The Knee voltage marks the point at which current transitions rapidly from reverse to forward bias, signifying the onset of light emission in OLEDs. Conversely, the breakdown voltage denotes the minimum reverse voltage at which the diode conducts current. The Knee voltage and breakdown voltage for these

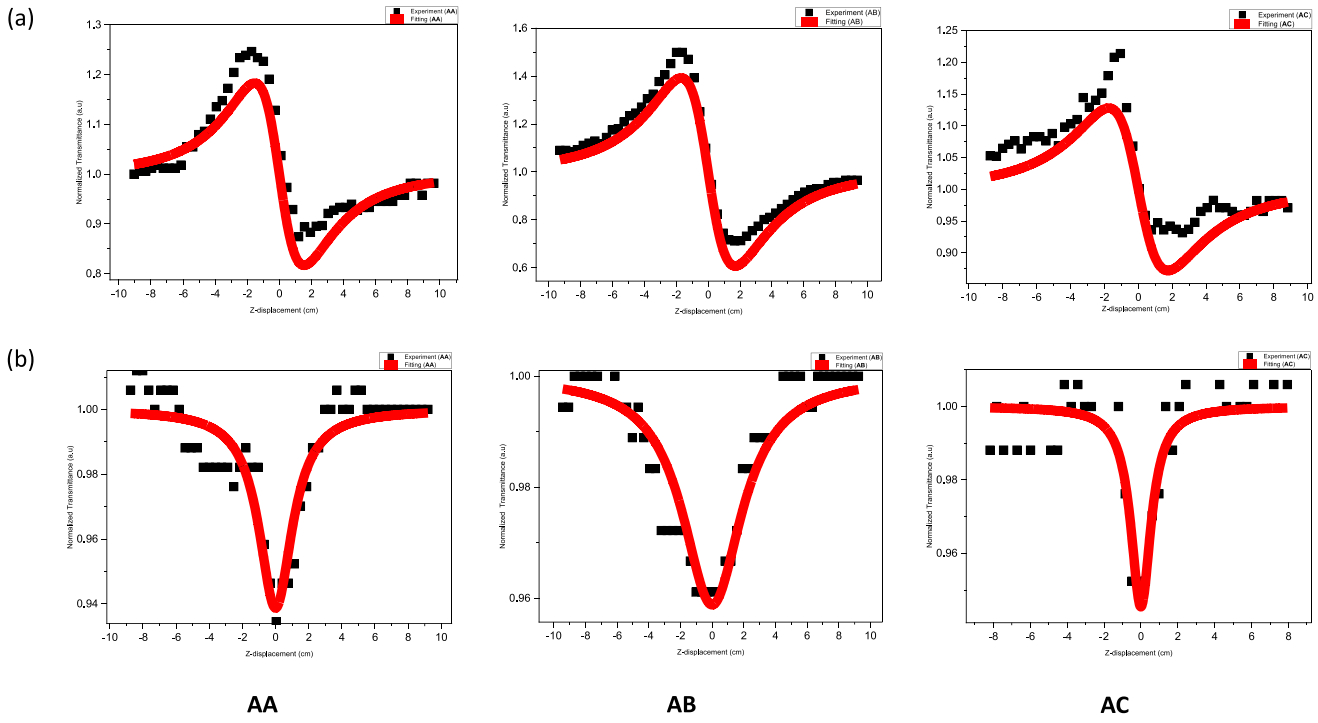

Fig. 10. (a) closed-aperture, (b) open-aperture Z-scan curves for fused aromatic chalcone derivatives (**AA, AB, AC**).

Table 8
Significant NLO parameters from Z-scan technique.

Compound	n_2 (x 10^{-11}cm^2/W)	Re $\chi^{(3)}$ (x 10^{-10} esu)	β (x 10^{-3} cm/W)	Im $\chi^{(3)}$ (x 10^{-5} esu)	$\chi^{(3)}$ (x 10^{-05} esu)
AA	4.66	3.37	1.30	1.50	1.50
AB	8.80	6.37	0.85	0.97	0.97
AC	3.40	2.46	1.15	1.30	1.30

fused aromatic chalcone derivatives are outlined in Table 9. These derivatives exhibit semiconductor properties facilitating current flow across the P-N junction, rendering them suitable for rectification applications like OLEDs[49].

Subsequently, the thin films were tested by passing through the direct current (DC) power supply to ITO substrate at different voltages of *circa* 15 V – 30 V to further investigate their light emitting ability. The intensities of light emission were observed from the ITO substrate as shown in Fig. 12, which showcases an increase in light emission with rising voltage and transitioning of light color from orange (15 V) to purple at (20 V– 30 V). It is expected to be attributed to the interference of suppression of electron injection from cathode to emissive layer leads to the interference of the light reflected from the layer boundaries resulting to the unstable color stability of light emission[50]. Hence, this study has proven all highly fused aromatic chalcones derivatives in this study have great potential as prospective OLEDs.

4. Conclusion

This comprehensive study illuminates the comparison of the chalcone system on both theoretical and experimental assessments of the highly fused aromatic structures constituting the synthesized chalcone derivatives. The standout discovery lies in the remarkably low energy

Table 9
The Knee voltage (V) and breakdown voltage (V) for highly fused aromatic chalcones (**AA, AB, AC**).

Compound	Knee Voltage (V)	Breakdown Voltage (V)
AA	3.2	−4.4
AB	3.2	−4.2
AC	2.4	−4.4

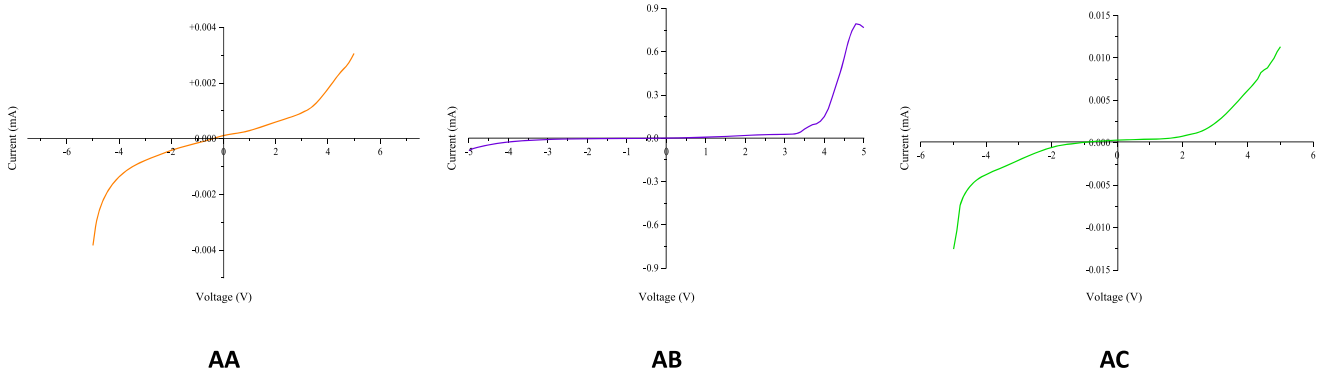

Fig. 11. The IV curve for highly-fused aromatic chalcone derivatives (**AA, AB, AC**).

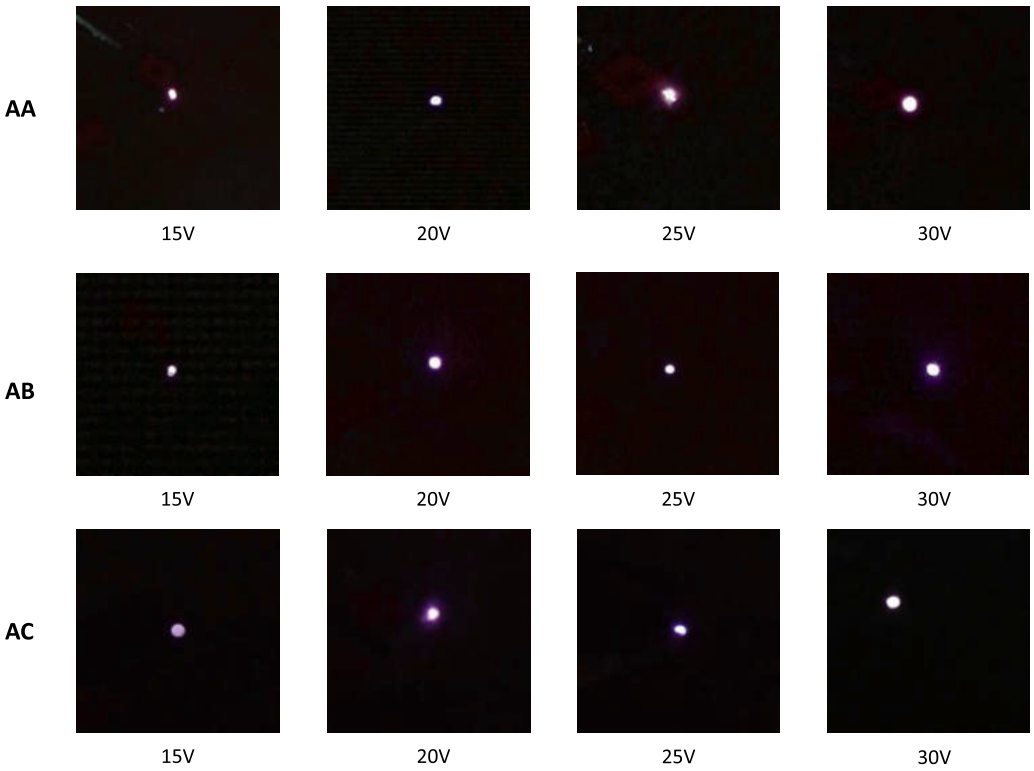

Fig. 12. The light emission with different voltages of fused aromatic chalcone derivatives (**AA, AB, AC**).

band gap, with **AC** exhibiting the lowest value at approximately 2.71 eV compared to its other derivatives. The lower energy band gap signifies the compound's ability to facilitate the transfer of a substantial number of electrons through π-conjugation. Furthermore, calculations support that **AC** has a distinction in having the highest value for electron affinity and electronegativity, indicating potent electron accepting and donating capabilities. These findings thus paved way for their future utilization in optoelectronic devices. The MEP mapping also highlighted all significant moieties as reactive sites that contributes to their reactivity. Moreover, it was proven that the compounds are thermally stable up to 200 °C, suggesting decomposition resilience during the fabrication stage, as well as hinting at a high thermal threshold – a crucial feature for NLO applications. All targeted compounds exhibit NLR activity within the range of $\chi(3)$ ($\sim \times 10^{-6}$ esu). **AC**, in particular, showcases the highest value of first order hyperpolarizability (β_{tot}) at 528.08 $\times$ 10^{-30} esu upon the substitution of strong electron acceptor. Evidently, the synthesized molecules demonstrated promising performance as conductive and emitting layers in OLED, demonstrating light-emitting ability at voltages as low as 15 V.

CRediT authorship contribution statement

Wan M. Khairul: Writing – review & editing, Supervision, Funding acquisition, Conceptualization. **Anisatul Aqidah Tagiling:** Writing – original draft, Methodology, Data curation. **Ain Qarina Muzaman:** Methodology. **Rafizah Rahamathullah:** Writing – review & editing, Validation, Methodology. **Mas Mohammed:** Writing – review & editing, Validation, Methodology. **Syaharil Saidin:** Validation, Methodology. **Suhana Arshad:** Writing – review & editing, Validation, Methodology. **Ibrahim Abdul Razak:** Validation, Conceptualization. **Fazira Ilyana Abdul Razak:** Writing – review & editing, Validation, Conceptualization. **Suhaila Sapari:** Writing – review & editing, Validation.

Declaration of competing interest

The authors declare that they have no known competing financial interests or personal relationships that could have appeared to influence the work reported in this paper.

Data availability

Data will be made available on request.

Acknowledgements

The authors would like to thank the Ministry of Higher Education, Malaysia for the Fundamental Research Grant Scheme, FRGS 59515 (FRGS/1/2018/STG07/UMT/02/6), Faculty of Science and Marine Environment, Universiti Malaysia Terengganu (UMT) for the Undergraduate Final Year Project allocations for student, Institute of Marine Biotechnology for NMR analysis and UMT in general for research facilities and support.

Supplementary materials

Supplementary material associated with this article can be found, in the online version, at doi:10.1016/j.molstruc.2024.139585.

References

[1] K. Boudhar, M. Debieche, A. Serhane, A. Zeghdaoui, Crystal structure, Raman spectroscopy study and quantum chemical DFT calculations of N-phenyl-3-para nitro phenyl isoxazolidine-5-carbonitrile, J. Mol. Struct. 1246 (2021) 131029, https://doi.org/10.1016/j.molstruc.2021.131029.

[2] H.A. Kurtz, J.J. Stewart, K.M. Dieter, Calculation of the nonlinear optical properties of molecules, J. Comput. Chem. 11 (1990) 82–87, https://doi.org/10.1002/jcc.540110110.

[3] S.R. Maidur, P.S. Patil, S.V. Rao, M. Shkir, S.M. Dharmaprakash, Experimental and computational studies on second-and third-order nonlinear optical properties of a novel D-π-A type chalcone derivative: 3-(4-methoxyphenyl)-1-(4-nitrophenyl) prop-

2-en-1-one, Opt. Laser Technol. 97 (2017) 219–228, https://doi.org/10.1016/j.optlastec.2017.07.003.
[4] J.C. Jebapriya, J.C. Prasana, U.M. Sumaya, P.S. Patil, Molecular structure and third-order non-linear optical properties of two novel tetralone-based chalcone derivatives: promising materials for optical limiting applications, J. Phys. Chem. Solid. 173 (2023) 111091, https://doi.org/10.1016/j.jpcs.2022.111091.
[5] F.L.S.A. Cuppo, A.M.F. Neto, S.L. Gómez, P. Palffy-Muhoray, Thermal-lens model compared with the Sheik-Bahae formalism in interpreting Z-scan experiments on lyotropic liquid crystals, JOSA B 19 (2002) 1342–1348, https://doi.org/10.1364/JOSAB.19.001342.
[6] P.S. Patil, M. Shkir, S.R. Maidur, S. AlFaify, M. Arora, S.V. Rao, H. Abbas, Ganesh V, Key functions analysis of a novel nonlinear optical D-π-A bridge type (2E)-3-(4-Methylphenyl)-1-(3-nitrophenyl) prop-2-en-1-one chalcone: an experimental and theoretical approach, Opt. Mater. 72 (2017) 427, https://doi.org/10.1016/j.optmat.2017.06.038. -235.
[7] T T. Unjaren, C. Kaivasuan, S. Arunlimsawat, P. Surawatanawong, T. Chantarojsiri, T. Sudyoadsuk, V. Promarak, N. Ruangsupapichat, Molecular design for high exciton utilization based donor-π-acceptor type fluorescent emitter for OLEDs application, Org. Electron. 120 (2023) 106848, https://doi.org/10.1016/j.orgel.2023.106848.
[8] K.S. Vishrutha, H. Ulla, B.R. Bhat, A.V. Adhikari, New green emitters based on push-pull type pyrene substituted cyanopyridones: design strategies and utilization in organic light-emitting diodes, Dye. Pigm. 219 (2023) 111560, https://doi.org/10.1016/j.dyepig.2023.111560.
[9] G. Chen, J. Wang, W.-C. Chen, Y. Gong, N. Zhuang, H. Liang, L. Xing, Y. Liu, S. Ji, H.-L. Zhang, Z. Zhao, Y. Huo, B.Z. Tang, Triphenylamine-functionalized multiple-resonance TADF emitters with accelerated reverse intersystem crossing and aggregation-induced emission enhancement for narrowband OLEDs, Adv. Funct. Mater. 33 (2023) 2211893, https://doi.org/10.1002/adfm.202211893.
[10] T. Sun, X. Shui, W. Chen, Y. Chen, W. Shi, J. Huang, B. Wei, Efficient and low roll-off deep-blue organic light-emitting diodes with anthracene-based compounds as hosts, New J. Chem. 48 (2024) 1867–1875, https://doi.org/10.1039/D3NJ04686A.
[11] S. Kagatikar, D. Sunil, D. Kekuda, M.N. Satyanarayana, S.D. Kulkarni, Y. N. Sudhakar, A.K. Vatti, A. Sadhanala, Pyrene-based chalcones as functional materials for organic electronics application, Mater. Chem. Phy. 293 (2023) 126839, https://doi.org/10.1016/j.matchemphys.2022.126839.
[12] B.-L. Yan, R. Sun, J.-F. Ge, D. Wang, H. Li, J.-M. L, Electronic memory devices based on the chalcone with negative electrostatic potential regions, Mater. Chem. Phys. 142 (2013) 363–369, https://doi.org/10.1016/j.matchemphys.2013.06.056.
[13] X. Feng, X. Wang, C. Redshaw, B.Z. Tang, Aggregation behaviour of pyrene-based luminescent materials, from molecular design and optical properties to application, Chem. Soc. Rev. 52 (2023) 6715–6753, https://doi.org/10.1039/D3CS00251A.
[14] W. Liu, S. Li, Z. Xie, K. Huang, K. Yan, Y. Zhao, C. Redshaw, X. Feng, B.Z. Tang, Molecular Engineering toward Broad Color-Tunable Emission of Pyrene-Based Aggregation-Induced Emission Luminogens, Adv. Opt. Mater. 12 (2024) 2400301, https://doi.org/10.1002/adom.202400301.
[15] D. Veselý, D. Yordanov, M. Vala, M. Weiter, J. Krajčovič, A. Georgiev, Acid-base fluorescence switching and aggregation induced emission (AIE) of phenylene-thienyl chalcones, J. Mol. Liq. 397 (2024) 124119, https://doi.org/10.1016/j.molliq.2024.124119.
[16] Y.P. Zhang, Q. Teng, Y.S. Yang, J.Q. Cao, J.J. Xue, Aggregation-induced emission properties of triphenylamine chalcone compounds, J. Fluoresc. 31 (2021) 807–815, https://doi.org/10.1007/s10895-021-02711-6.
[17] R.G.M. da Costa, R. dos Santos Carvalho, V.G. Isoppo, A.R.J. Barreto, M.J. P. Peñafiel, A.M. dos Santos, D. Back, R.Q. Aucélio, M. Cremona, F.S. Rodembusch, J. Limberger, Aryloxy-benzothiadiazole-chalcone and aryloxy-benzothiadiazole-fluorene AIEE luminogens: synthesis, photophysical properties, and electroluminescence evaluation, Dye. Pigm. 219 (2023) 111533, https://doi.org/10.1016/j.dyepig.2023.111533.
[18] A.R. Nair, C. Raksha, R. Heera, M.G. Mohan, P. Manoj, A. Sivan, D-A-D/A chalcones with tunable optical characteristics: synthesis, photophysical, electrochemical and theoretical investigations, J. Photochem. Photobiol., A. 451 (2024) 115511, https://doi.org/10.1016/j.jphotochem.2024.115511.
[19] S.R. Shankara, K.M. Eshwarappa, A. Jayarama, S. Prabhu, R. Pinto, Enhancing nonlinear optical responses via Methoxy Positional Isomerism in Chalcone-Based Materials, Mater. Chem. Phys. 312 (2024) 128662, https://doi.org/10.1016/j.matchemphys.2023.128662.
[20] K.Y. Teo, M.H. Tiong, H.Y. Wee, N. Jasin, Z.Q. Liu, M.Y. Shiu, J.Y. Tang, J.K. Tsai, R. Rahamathullah, W.M. Khairul, M.G. Tay, The influence of the push-pull effect and a π-conjugated system in conversion efficiency of bis-chalcone compounds in a dye sensitized solar cell, J. Mol. Struct. 1143 (2017) 42–48, https://doi.org/10.1016/j.molstruc.2017.04.059.
[21] W.M. Khairul, M. Mohammed, R. Rahamathullah, M.F. Zaini, S. Arshad, A. R. Ibrahim, F.I.A. Razak, S. Sapari, Deciphering ethynyl single crystal for NLO applications: synergistic studies on the structural, Hirshfeld surface, photophysical and DFT assessment, Opt. Mater. 147 (2024) 114726, https://doi.org/10.1016/j.optmat.2023.114726.
[22] A.E.M. Abdallah, S.A. Abdel-Latif, G.H. Elgemeie, Novel fluorescent benzothiazolyl-coumarin hybrids as anti-SARS-COVID-2 agents supported by molecular docking studies: design, synthesis, X-ray crystal structures, DFT, and TD-DFT/PCM calculations, ACS Omega 22 (2023) 19587–19602, https://doi.org/10.1021/acsomega.3c01085, 8.
[23] W. Omara, S.A. Abdel-Latif, H.M.E. Azzazy, N.S. Abdel-Kader, Exploring polyaniline nanofilaments for enhanced optical recognition of lead in water: an integrated approach of experimental and theoretical studies, Appl. Organomet. Chem. 38 (2024) 7439, https://doi.org/10.1002/aoc.7439.
[24] O.A. Abbas, O.M. El-Roudi, S.A. Abdel-latif, Novel 1, 3-diphenyl-4-(N, N-dimethylimido dicarbonimidic diamide azo)-5-pyrazolone and its chelates with manganese, nickel, copper, and zinc divalent metal ions as an antibacterial activity supported by molecular docking studies: design, synthesis, DFT, and TD-DFT/PCM calculations, Appl. Organomet. Chem. 37 (2023) 7236, https://doi.org/10.1002/aoc.7236.
[25] V.S. Naik, P.S. Patil, Q.A. Wong, C.K. Quah, N.B. Gummagol, H.S. Jayanna, Molecular structure, linear optical, second and third-order nonlinear optical properties of two non-centrosymmetric thiophene-chalcone derivatives, J. Mol. Struct. 1222 (2020) 128901, https://doi.org/10.1016/j.molstruc.2020.128901.
[26] A.N. Ekbote, S.R. Maidur, J.R. Jahagirdar, P.S. Patil, V.R. Soma, Femtosecond nonlinear optical investigations of nitro chalcones-doped PMMA thin films for optical limiting and photonic applications, Mater. Today Commun. 37 (2023) 107240, https://doi.org/10.1016/j.mtcomm.2023.107240.
[27] J.R. Jahagirdar, S.R. Maidur, P.S. Patil, T.S. Chia, C.K. Quah, Growth, characterizations and nonlinear optical studies of dimethylamine substituted anthracene chalcone single crystals, J. Mol. Struct. 1278 (2023) 134897, https://doi.org/10.1016/j.molstruc.2022.134897.
[28] S.K. Alsaee, M.A.A. Bakar, D.A. Zainuri, A.H. Anizaim, M.F. Zaini, M.M. Rosli, M. Abdullah, S. Arshad, I.A. Razak, Nonlinear optical properties of pyrene-based chalcone: (E)-1-(4′-bromo-[1,1′-biphenyl]-4-yl)-3-(pyren-1-yl)prop-2-en-1-one, a structure-activity study, Opt. Mater. 128 (2022) 112314, https://doi.org/10.1016/j.optmat.2022.112314.
[29] T.P. Phan, K.Y. Teo, Z.Q. Liu, J.K. Tsai, M.G. Tay, Application of unsymmetrical bis-chalcone compounds in dye sensitized solar cell, Chem. Data Coll. 20 (2019) 100256, https://doi.org/10.1016/j.cdc.2019.100256.
[30] A. Suvitha, S. Periandy, S. Boomadevi, M. Govindarajan, Vibrational frequency analysis, FT-IR, FT-Raman, ab initio, HF and DFT studies, NBO, HOMO-LUMO and electronic structure calculations on pycolinaldehyde oxime, Spectrochim. Acta A Mol. Biomol. Spectrosc. 117 (2014) 216–224, https://doi.org/10.1016/j.saa.2013.07.080.
[31] d C.E.S. Nogueira, M.M. de Oliveira, A.M.R. Teixeira, P.N. Bandeira, H.S. dos Santos, A.P. Ayala, B.P. Bezerra, A.C.H. Barreto, P.T.C. Freire, Crystal structure, FT-Raman and FTIR spectra and DFT calculations of chalcone (2E)-1-(4-aminophenyl)-3-(furan-2-yl)prop-2-en-1-one monohydrate, J. Mol. Struct. 1212 (2020) 128141, https://doi.org/10.1016/j.molstruc.2020.128141.
[32] S.T. Lee, W.M. Khairul, O.J. Lee, R. Rahamathullah, A.I. Daud, K.H.K. Bulat, S. Sapari, F.I.A. Razak, G. Krishnan, Electronic, reactivity and third order nonlinear optical properties of thermally-stable push-pull chalcones for optoelectronic interest: experimental and DFT assessments, J. Phys. Chem. Solids. 159 (2021) 110276, https://doi.org/10.1016/j.jpcs.2021.110276, 2021.
[33] P.R. Buvaneswari, M.S.J.S. Raj, K. Sudha, T. Aravind, P. Chakkaravarthy, M. Raja, Comprehensive analysis of (E)-3-(4-chlorophenyl)-1-(4-methoxyphenyl)prop-2-en-1-one (4CP4MPO): synthesis, Spectroscopic, salvation electronic properties, electron-hole transition, topological, Hirshfeld surface and molecular docking analysis, Chem. Phys. Impact. 8 (2024) 100452, https://doi.org/10.1016/j.chphi.2023.100452.
[34] Z. Ngaini, N.I.A Rahman, Synthesis and characterization of cyclotriphosphazenes bearing chalcones derivatives, Phosph. Sulf. Silicon Relat. Elem. 185 (2010) 628–633, https://doi.org/10.1080/10426500902893217.
[35] S. Mary, C.Y. Panicker, P.L. Anto, M. Sapnakumari, B. Narayana, B.K. Sarojini, Molecular structure, FT-IR, NBO, HOMO and LUMO, MEP and first order hyperpolarizability of (2E)-1-(2,4-Dichlorophenyl)-3-(3,4,5-trimethoxyphenyl) prop-2-en-1-one by HF and density functional methods, Spectrochim. Acta. A Mol. Biomol. Spectrosc. 135 (2015) 81–92, https://doi.org/10.1016/j.saa.2014.06.140.
[36] S. Saeed, N. Rashid, P.G. Jones, M. Ali, R. Hussain, Synthesis, characterization and biological evaluation of some thiourea derivatives bearing benzothiazole moiety as potential antimicrobial and anticancer agents, Eur. J. Med. Chem. 45 (2010) 1323–1331, https://doi.org/10.1016/j.ejmech.2009.12.016.
[37] A. Karuppusamy, A. Sharma, K.J. Thomas, P. Kannan, Experimental and theoretical investigations on chalcones containing pyrene, J. Mol. Struct. 1268 (2022) 133532, https://doi.org/10.1016/j.molstruc.2022.133532.
[38] R.Y. Iliashenko, N.Y. Gorobets, A.O. Doroshenko, New and efficient high Stokes shift fluorescent compounds: unsymmetrically substituted 1, 2-bis-(5-phenyloxazol-2-yl) benzenes via microwave-assisted nucleophilic substitution of fluorine, Tetrahedron Lett. 52 (2011) 5086–5089, https://doi.org/10.1016/j.tetlet.2011.07.100.
[39] G. Yakali, A. Bicer, C. Eke, G.T. Cin, Solid state structural investigations of the bis (chalcone) compound with single crystal X-ray crystallography, DFT, gamma-ray spectroscopy and chemical spectroscopy methods, Radiat. Phys. Chem. 145 (2018) 89–96, https://doi.org/10.1016/j.radphyschem.2017.12.002.
[40] R. Raju, C.Y. Panicker, P.S. Nayak, B. Narayana, B.K. Sarojini, C. Van Alsenoy, A. A. Al-Saadi, FT-IR, molecular structure, first order hyperpolarizability, MEP, HOMO and LUMO analysis and NBO analysis of 4-[(3-acetylphenyl)amino]-2-methylidene-4- oxobutanoic acid, Spectrochim. Acta A Mol. Biomol. Spectrosc. 134 (2015) 63–72, https://doi.org/10.1016/j.saa.2014.06.051.
[41] C.Y. Panicker, H.T. Varghese, P.S. Nayak, B. Narayana, B.K. Sarojini, H.K. Fun, J. A. War, S.K. Srivastava, C. Van Alsenoy, Infrared spectrum, NBO, HOMO-LUMO, MEP and molecular docking studies (2E)-3-(3-nitrophenyl)-1-[4-piperidin-1-yl] prop-2-en-1-one, Spectrochim. Acta A Mol. Biomol. Spectrosc. 148 (2015) 18–28, https://doi.org/10.1016/j.saa.2015.03.065.
[42] F. Cheng, Y. Yin, G. Zhang, Y. Wang, W. Deng, F. Wu, Optoelectronic and thermal properties of highly fluorescence emissive 2, 2′-distyryl-[3, 3′]-bithiophenes, Dye. Pigm. 140 (2017) 222–228, https://doi.org/10.1016/j.dyepig.2017.01.042.

[43] A. Solmaz, Z. İlter, İ. Kaya, Synthesis, characterization, thermal and kinetic properties of chalcone methacrylamide polymers containing halogen group in side chain, Polym. Bull. 79 (2022) 5041–5061, https://doi.org/10.1007/s00289-021-03733-7.

[44] D. Sajan, J. Binoy, I.H. Joe, V.S. Jayakumar, J. Zaleski, Vibrational spectral studies of methyl 3-(4-methoxyphenyl)prop-2-enoate, a new organic non-linear optic crystal, J. Raman Spectrosc. 36 (2005) 221–236, https://doi.org/10.1002/jrs.1279.

[45] K. Thanigaimani, S. Arshad, N.C. Khalib, I.A. Razak, C. Arunagiri, A. Subashini, S. F. Sulaiman, N.S. Hashim, K.L. Ooi, A new chalcone structure of (E)-1-(4-Bromophenyl)-3-(napthalen-2-yl)prop-2-en-1-one: synthesis, structural characterizations, quantum chemical investigations and biological evaluations, Spectrochim. Acta A Mol. Biomol. Spectrosc. 149 (2015) 90–102, https://doi.org/10.1016/j.saa.2015.04.028.

[46] S.R. Maidur, J.R. Jahagirdar, P.S. Patil, T.S. Chia, C.K. Quah, Structural characterizations, Hirshfeld surface analyses, and thirdorder nonlinear optical properties of two novel chalcone derivatives, Opt. Mater. 75 (2018) 580–594, https://doi.org/10.1016/j.optmat.2017.11.008.

[47] T.H. Clara, D.R. Jonathan, R. Ragu, M. NizamMohideen, J.C. Prasana, Crystal structure, physico-chemical and third order nonlinear traits of the novel (2E)-1-(3,4-dimethoxyphenyl)-3-(4-propoxyphenyl) prop-2-en-1-one (DMPP) chalcone single crystal, J. Solid State Chem. 302 (2021) 122382, https://doi.org/10.1016/j.jssc.2021.122382.

[48] S.M. Jasman, W.M. Khairul, T. Tagg, K. KuBulat, R. Rahamathullah, S. Arshad, I. A. Razak, M.I.M. Tahir, Synthesis, crystal structure and electrical studies of Naphthoyl-Thiourea as potential organic light emitting diode, J. Chem. Crystallogr. 45 (2015) 338–349, https://doi.org/10.1007/s10870-015-0599-6.

[49] K.S. Karimov, M. Abid, Applications of nano materials, organic semiconductor complexes and composites based devices, Nanomater. Fascinat. Attribut. 1 (2016) 91.

[50] K.S. Daskalakis, F. Freire-Fernández, A.J. Moilanen, S. Van Dijken, P. Törmä, Converting an organic light-emitting diode from blue to white with Bragg modes, ACS Photon. 6 (2019) 2655–2662, https://doi.org/10.1021/acsphotonics.9b01206.